



Review

# A Short Survey on Lung Cancer Diagnosis Based on CT Imaging and Artificial Intelligence

Baihua Zhang<sup>1,\*</sup> and Yu Wang<sup>2</sup><sup>1</sup> Research Institute for Medical and Biological Engineering, Ningbo University, Ningbo 315211, China<sup>2</sup> School of Medical Imaging, Wannan Medical College, Wuhu 241000, China

\* Correspondence: zhangbaihua@nbu.edu.cn

**How To Cite:** Zhang, B.; Wang, Y. A Short Survey on Lung Cancer Diagnosis Based on CT Imaging and Artificial Intelligence. *AI Medicine* 2025, 2(2), 9. <https://doi.org/10.53941/aim.2025.100009>

Received: 15 October 2025

Revised: 20 November 2025

Accepted: 5 December 2025

Published: 9 December 2025

**Abstract:** Lung cancer is one of the most prevalent and lethal malignant tumors globally, characterized by high morbidity and mortality rates. Early diagnosis is crucial for enhancing treatment efficacy, reducing mortality, and improving patients' quality of life. Traditional manual interpretation of computed tomography (CT) images—the primary screening tool for lung cancer—is often limited by subjectivity, heavy workload, and potential missed diagnoses. Artificial Intelligence (AI) methodologies have emerged as indispensable assets for radiologists, empowering them to conduct in-depth analyses of lung CT scans. This technology facilitates a more streamlined and unbiased evaluation of anatomical structures and pathological features depicted in chest CT images. Driven by advances in deep learning models such as convolutional neural networks (CNNs), the accuracy and robustness of AI methods for lung cancer diagnosis have been significantly improved, providing reliable references for clinical practice. This paper presents a brief review of the applications of AI methods in lung cancer diagnosis based on CT imaging in recent years. It systematically organizes and elaborates on the applications of AI methods represented by deep learning in pulmonary nodule detection, lung tumor segmentation, benign-malignant classification of lung cancer, and lung cancer-related gene mutation detection. Additionally, it analyzes the performance of different models on relevant datasets. Furthermore, the limitations of AI in CT imaging-based lung cancer diagnosis and future research directions are summarized. Through this survey, we aim to provide a concise and comprehensive overview of the current status of lung cancer diagnosis using CT-AI integrated systems, and ultimately promote the development and clinical application of these technologies in the early and accurate detection of lung cancer.

**Keywords:** lung cancer; computed tomography; artificial intelligence; epidermal growth factor receptor

## 1. Introduction

Lung cancer is one of the malignant tumors with extremely high incidence and mortality rates globally, as well as in China. It is the leading cause of cancer-related deaths worldwide, with 2.5 million new diagnoses and 1.8 million deaths annually [1]. Its overall prognosis is poor, and the 1-year survival rate of patients with advanced lung cancer is approximately 33% [2]. The high incidence and mortality rates of lung cancer pose severe challenges to global public health [1]. In China, lung cancer is the leading cause of new cancer cases and deaths, which may be attributed to the high prevalence of smoking. Lung cancer ranks first among the most prevalent cancers in China; it was the most common cancer in 2022 (1,060,600 cases). For both sexes combined, lung cancer was the leading cause of cancer death (733,300 deaths). During 2000–2018, the Age-Standardized Incidence Rate (ASIR)



**Copyright:** © 2025 by the authors. This is an open access article under the terms and conditions of the Creative Commons Attribution (CC BY) license (<https://creativecommons.org/licenses/by/4.0/>).

**Publisher's Note:** Scilight stays neutral with regard to jurisdictional claims in published maps and institutional affiliations.

also showed an increase for cancers of the uterus (3.4%) and lung (3.1%). During 2014–2018, the ASIR of lung cancer (2.7%) showed a significant increase in males. These data fully indicate that lung cancer remains a key priority in the prevention and treatment of malignant tumors in China [3].

Lung cancer originates from respiratory epithelial cells and is primarily classified into two histological types: non-small cell lung cancer (NSCLC), which accounts for 80–85% of cases, and small cell lung cancer (SCLC), comprising 10–15% of cases [4]. The classification of lung cancer subtypes is shown in Figure 1. According to the 2021 WHO Classification of Lung Tumors [5], common subtypes include adenocarcinoma, squamous cell carcinoma, and neuroendocrine tumors [6]. Both NSCLC and SCLC impose substantial financial burdens on patients and society, underscoring lung cancer's significant public health impact and the impediment it represents to human progress and socioeconomic development [3].

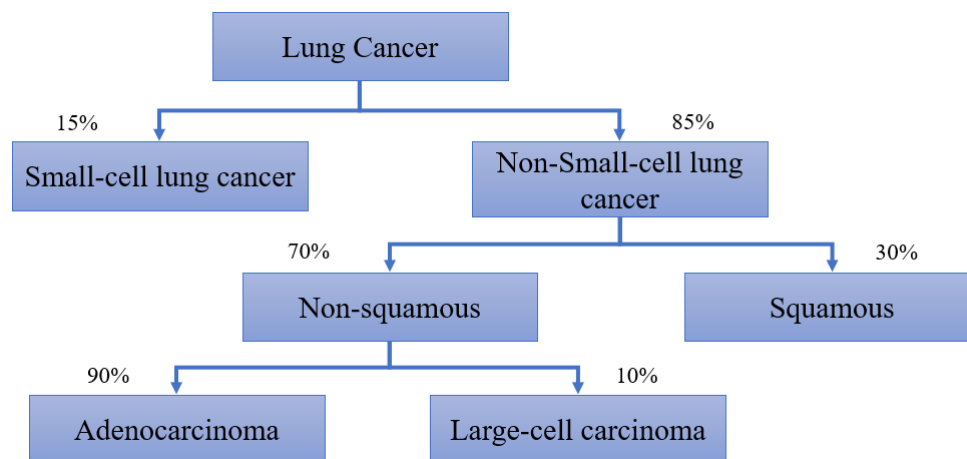


**Figure 1.** Classification of lung cancer subtypes.

The imaging features of lung cancer range from a single tiny nodule to ground-glass opacity, multiple nodules, pleural effusion, lung collapse, and multiple opacities [7]; simple and small lesions are extremely difficult to detect [8]. Comprehensive management throughout the entire course of lung cancer patients can improve survival rates; therefore, early screening and diagnosis of lung cancer are also topics of common concern in current clinical and research fields [9].

Computed Tomography (CT) is an X-ray-based imaging technique that enables high-resolution, high-contrast non-invasive scanning of the internal human body. As a commonly used screening imaging modality in medicine, CT has achieved considerable success in detecting early-stage cancers; specifically, chest CT provides a non-invasive method for examining the three-dimensional structure of the thoracic cavity. With advancements in technology, radiation exposure associated with CT scans has been significantly reduced compared to that in previous years. Chest CT remains the cornerstone of lung cancer diagnostics [10–12]. However, the traditional manual imaging diagnosis model has certain limitations, and these limitations pose a significant obstacle to the comprehensive analysis of data captured during screening. First, a single chest CT scan can generate 300 to 500 cross-sectional images. Radiologists are required to analyze this large volume of images for an individual patient within a limited time frame, and prolonged work easily leads to fatigue, which impairs diagnostic accuracy [13]. Second, when it comes to multiple pulmonary nodules and tiny pulmonary nodules, the limitations of human visual resolution often led to misdiagnoses and missed diagnoses. Finally, diagnosis relies on the personal experience of radiologists, so significant discrepancies may exist in diagnostic opinions among radiologists with different years of clinical experience. Additionally, primary hospitals may face challenges such as a shortage of specialist physicians and suboptimal radiological equipment, which can further compromise diagnostic accuracy.

Artificial Intelligence (AI) refers to a technological system that simulates human cognitive functions through computer systems. Its core features include pattern recognition, decision-making, and autonomous learning capabilities. Additionally, AI can create mathematical models that establish connections between different types of information, which are used to predict or classify objects [14]. Its main components include datasets for training, preprocessing methods, algorithms for generating predictive models, and pre-trained models—these pre-trained models serve to accelerate model construction and leverage prior experience. Machine learning (ML) is a subset of artificial intelligence, which includes decision trees (DT), support vector machines (SVM), and Bayesian networks (BN). In contrast, deep learning is another subset derived from the neural network approach within machine learning [15]. Unlike radiomics methods that rely on manually predefined features, deep learning can

automatically extract high-dimensional features through large-scale training, thus exhibiting greater adaptability and generalization potential.

With the development of artificial intelligence (AI) technology, especially methods represented by deep learning, its application in medical scenarios combined with CT images has become widespread. Since the 21st century, human life has been largely integrated with AI, and this trend has also extended to the medical field. In the field of medical imaging, AI has demonstrated significant advantages: it can not only effectively address time-consuming diagnostic tasks (e.g., improving the accuracy of lesion measurement) but also compensate for the limitations of physicians' visual observation. By extracting in-depth information from images through algorithms, AI enhances diagnostic and predictive efficiency, and in some studies, it has shown diagnostic accuracy comparable to or higher than that of human experts [16]. Specifically, it has made important progress in the fields of tumor screening, diagnosis, and treatment [17]. These applications have improved the accuracy and efficiency of imaging diagnosis, providing physicians with more reliable auxiliary diagnostic tools. Additionally, AI can accelerate the speed of problem detection, improve diagnostic accuracy, and assist in formulating personalized treatment plans in the healthcare field.

The implementation of artificial intelligence (AI) has been one of the most impactful changes in the field of lung cancer CT image diagnosis over the past decade [18]. The number of relevant studies has grown exponentially, driven primarily by breakthroughs in AI algorithms, the establishment of high-quality medical imaging databases, and the continuous impetus of clinical translation needs. Meanwhile, the heterogeneity of lung cancer makes it a key area for AI applications, including lung cancer prevention [19] and the development of early screening models based on lung cancer epidemiology and clinical characteristics [20]. AI has been applied to various imaging modalities [21,22], such as CT [10]. AI methods have also yielded remarkable achievements in the field of differentiating Tuberculosis (TB) and pneumonia. Lu et al. proposed a novel deep learning framework—Large Adaptive Filter and Alignment Normalization Network (LAFAN-Net)—which can extract clinically meaningful features while maintaining interpretability [23]. In another study, Lu et al. applied the improved Transformer model to TB classification and conducted experiments on both private and public datasets, verifying the advancement of their proposed CTBViT classification method [24]. Regarding pneumonia prediction, Zhu et al. [25] proposed a new method, OPT-CO, which achieves efficient COVID-19 classification without significantly increasing parameters and evaluated the performance of the proposed model on multiple datasets. Meanwhile, Zhu et al. [26] proposed the Large Kernel Adapter (LKA) method, applying the improved Parameter-Efficient Fine-Tuning (PEFT) method to Tuberculosis and pneumonia datasets and achieving satisfactory results. Furthermore, AI also helps improve various diagnostic methods, such as bronchoscopy [27] and cancer staging [28]. In the field of lung cancer prediction, several studies have achieved positive results [29–31], demonstrating that deep learning methods can be well applied to CT image-based lung cancer diagnosis. In summary, deep learning-driven AI technology has demonstrated unique advantages in lung cancer screening, prediction, and treatment. It can help radiologists reduce workload, minimize diagnostic uncertainty, and improve screening efficiency, thus emerging as a key direction to break through the bottlenecks of current precision diagnosis and treatment. Additionally, it provides a solid theoretical basis for identifying multi-omics biomarkers associated with lung cancer prognosis and establishing a precision diagnosis and treatment system for lung cancer. From the perspective of clinical practice, this study systematically explores the application progress of AI in lung cancer CT image diagnosis. CT image-based diagnosis is mainly divided into four aspects: lung cancer detection, lung tumor segmentation, benign-malignant prediction of pulmonary nodules, and lung cancer-related gene mutation prediction, as shown in Figure 2.

During our review process, we identified four relevant studies focusing on the intersection of radiomics and deep learning in lung cancer (LC). Chiu et al. [32] systematically summarized the applications of artificial intelligence (AI) methods in lung cancer research based on low-dose computed tomography (LDCT), chest X-ray (CXR), and pathological sections. By predicting tumor characteristics, treatment responses, side effects, and prognosis, these methods provide support for clinicians' decision-making. Kotoulas et al. [33] reviewed the applications of AI over the past 5 to 10 years in distinguishing benign from malignant pulmonary nodules, identifying biomarkers, and specific genetic markers critical to disease treatment across various imaging modalities, such as chest X-ray, computed tomography (CT), and positron emission tomography (PET). Huang et al. [34] outlined the limitations and translational potential of AI and radiomics technologies in tumor diagnosis and treatment supported by key imaging modalities including computed tomography (CT), magnetic resonance imaging (MRI), and positron emission tomography (PET), and highlighted their prospects in optimizing cancer diagnosis, prognostic assessment, and treatment outcomes in the future. Ayasa et al. [35] summarized the applications and challenges of AI technologies, including machine learning and deep neural networks, in lung cancer diagnosis and treatment based on different imaging modalities, with a focus on early diagnosis and personalized therapy.



intravenous contrast using the GE Lightspeed CT scanner, and radiation oncologists contoured the primary tumor site using soft tissue and lung windows. The NSCLC-Radiomics collection includes images from 422 non-small cell lung cancer (NSCLC) patients. For these patient's pretreatment CT scans, manual delineation of the 3D volume of the gross tumor volume by a radiation oncologist and relevant clinical outcome data are available. This dataset corresponds to the Lung1 dataset. The National Lung Screening Trial (NLST) enrolled 53,454 high-risk individuals for lung cancer from 33 U.S. medical centers between August 2002 and April 2004. Participants were randomly assigned to undergo three annual screenings with either low-dose CT or single-view posteroanterior chest radiography. This dataset includes low-dose CT scans from 26,254 of these participants, as well as digitized histopathology images from 451 subjects. LUNA16 is a curated version of the LIDC-IDRI dataset, consisting of 888 diagnostic and lung cancer screening thoracic CT scans obtained from seven academic centers and eight medical imaging companies, with a total of 1186 nodules. The nodules are accompanied by annotations agreed upon by at least three out of four radiologists. In addition to nodule location annotations, radiologists also documented various observed attributes, such as internal composition, calcification, malignancy, and suspiciousness. The LUNA25 dataset comprises 2120 patients and 4069 low-dose chest CT scans, including 555 annotated malignant nodules and 5608 benign nodules. The comparison of different datasets is presented in Table 1.

**Table 1.** Public CT datasets related to lung cancer diagnosis.

Dataset Name	Image Modality	Number of Images	Label	Description/Specifics	Citation/Link
LIDC-IDRI	CT	1018	Nodule location by four radiologists	A dataset that identifies as completely as possible all lung nodules in each CT scan without requiring forced consensus.	[36]
HarvardRT	CT	317	The primary tumor site	a cohort of 317 patients with stage I–IIIB NSCLC treated with radiation therapy between 2001 and 2015.	[37]
NSCLC-Radiomics	CT	422	3D volume of the gross tumor volume	This collection contains images from 422 non-small cell lung cancer patients and refers to the Lung1 dataset.	<a href="https://www.cancerimagingarchive.net/collection/nsclc-radiomics/">https://www.cancerimagingarchive.net/collection/nsclc-radiomics/</a> (accessed on 20 November 2025)
NLST	CT	26,254	Histopathology, Demographic, Diagnosis	From August 2002 through April 2004, Participants were randomly assigned to undergo three annual screenings with either low-dose CT.	[38]
LUNA 16	CT	888	Nodule location annotations, Malignancy	a curated version of the LIDC-IDRI dataset of 888 diagnostic and lung cancer screening thoracic CT scans obtained.	[39]
LUNA 25	CT	6163	Location annotations, Malignancy	The LUNA25 challenge training dataset consists of over 6163 nodules from the NLST trial, acquired between 2002–2004.	<a href="https://luna25.grand-challenge.org/">https://luna25.grand-challenge.org/</a> (accessed on 20 November 2025)

### 3. AI in CT Image-Based Pulmonary Nodule Detection

Pulmonary nodule detection is one of the most widely studied applications in the field of medical imaging. Currently, relatively mature results have been achieved, and some lung cancer screening tasks have been reported to yield favorable outcomes [10,40–42]; in particular, pulmonary nodule detection software can also achieve good detection performance [43]. Deep learning algorithms can automatically detect small pulmonary nodules in CT images, with a sensitivity of 96.7%—which is significantly higher than that of traditional radiologists (78.1%)—and they reduce the image reading time from 30 to 60 min to several minutes. AI is expected to improve the early detection rate and reduce the false positive rate in large-scale screening [44].

The resolution of CT images has a significant impact on pulmonary nodule detection. Jiang et al. confirmed that the pulmonary nodule detection rate of the computer-aided diagnosis (CAD) system using a  $1024 \times 1024$  high-resolution matrix was significantly superior to that of the system using the traditional  $512 \times 512$  matrix [45,46]. When Park et al. used software to detect subsolid nodules, the sensitivity reached as high as 92%. Existing studies have confirmed that image resolution has a significant impact on detection performance [47]. The fully automated lung cancer detection system developed by Primakov et al. based on 1328 chest CT scan datasets achieved an area under the receiver operating characteristic curve (AUC) of 0.98 in the external validation set, with a sensitivity of 0.97 and a specificity of 0.99 [48]. Meanwhile, leveraging artificial intelligence (AI) to screen large volumes of pulmonary images obtained for non-cancerous reasons can facilitate the easy and early identification of incidental pulmonary nodules (IPNs), which might otherwise have been missed [21].

Different deep learning models have been applied in research on pulmonary nodule detection. Liu et al. proposed a deep multi-task learning (MTL) approach to integrate these tasks for improved lung nodule detection. Lung nodule detection is performed in an anchor-free manner by dividing it into two subtasks: nodule center identification and nodule size regression [49]. A cascaded multi-stage framework proposed by Zhou et al. achieved

a nodule detection sensitivity of 95.95% on the LUNA16 dataset [50]. Han et al. adopted a two-stage approach that combines the advantages of 3D-RPN and U-Net for pulmonary nodule detection; the detected nodules are then fed into a ResNet classifier for classification [51]. Song et al. proposed a multiscale 3D anchor-free deep learning network (M3N) for pulmonary nodule detection, leveraging adjustable nodule modeling (ANM). Experimental results show that M3N achieves a competitive performance metric (CPM) of 90.6% on the LUNA16 dataset [52]. Bhatia et al. proposed a continuous learning-based deep neural network that can be applied to both labeled and unlabeled data to improve efficiency. It enables ultra-sensitive, specific, and accurate early detection of lung cancer [53]. Karimullah et al. addressed the pressing need for early detection through a novel diagnostic approach that leverages innovative image processing techniques, using the CBO+DenseNet CNN. Notable enhancements were observed in accuracy (98.17%), specificity (97.32%), precision (97.46%), and recall (97.89%) [54].

Some object detection models widely used in natural images have been improved and applied to pulmonary nodule detection. Huang et al. introduced the 3D OSAF-YOLOv3 model for pulmonary nodule detection, which was developed by integrating the 3D YOLOv3 architecture with a one-shot aggregation module, a receptive field block, and a feature fusion scheme [55]. Xu et al. proposed an improved Faster R-CNN model. On the basis of Faster R-CNN, a multi-scale training strategy is used to fully mine features across different scale spaces, and path augmentation is performed on lower-dimensional features—this improves the model’s small object detection ability, with the performance increasing from 76.4% to 90.7% [56]. Cai et al. proposed an artificial intelligence-based anti-interference lung nodule detection method primarily structured with YOLOv8, which integrates the adaptive gating sparse attention (AGSA) and Haar wavelet downsampling (HWD) modules, referred to as YOLOv8-AH. It achieves a 24% improvement in mAP50 and an 8.2% improvement in precision [57]. Zamanidoost et al. presented an improved Faster R-CNN by introducing an optimized multi-scale convolutional neural network (OMS-CNN). The results demonstrate that the OMS-CNN technique effectively extracts representative features of nodules of various sizes, achieving a sensitivity of 94.89% and a CPM score of 0.892 [58].

Although a British study shows that AI excluded negative cases [59], existing commercial detection software still has a certain false positive rate [60]. To reduce unnecessary follow-up examinations, future research on detection needs to continue improving in aspects such as reducing the false positive rate.

A summary of the methods mentioned above is given in Table 2.

**Table 2.** AI and CT image-based pulmonary nodule detection methods.

Author	Model	Dataset	Result	Core Innovations of the Study	Definition of Key Experimental Indicators
Park et al. (2021) [47]	Deep learning-based CAD and super-resolution algorithm	308 patients with 424 SSNs	SSN detection: 0.92 (1-mm) nonsolid nodules: 0.78 (1-mm)	Proposed a deep learning-based super-resolution algorithm to convert 5-mm thick CT images into 1-mm thick.	AUC; Sensitivity
Liu et al. (2021) [49]	Deep multi-task learning (MTL) network	LUNA16 dataset	increase the accuracy of lung segmentation and nodule detection, from 0.927/0.980 to 0.939/0.988	present a novel pyramid dilated convolution block (PDCB) for nodule detection method.	Sensitivity; FPs/scan; Dice similarity coefficient (DSC)
Primakov et al. (2022) [48]	Fully automated pipeline for NSCLC detection	1328 thoracic CT scans from 8 institutions	sensitivity of 0.97 and specificity of 0.99 in the external validation dataset and AUC of 0.98.	compared the detection efficiency and reproducibility of AI with human experts.	Dice similarity coefficient (DSC); receiver operating characteristic curve (AUC)
Huang et al. (2022) [55]	3D OSAF-YOLOv3	LUNA-16 dataset (888 LDCT scans)	Sensitivity: 0.962; CPM: 0.905.	Based on the 3D YOLOv3 framework, introduced a one-shot aggregation (OSA) module.	CPM (Competition Performance Metric); Sensitivity; False Positive Rate
Zhou et al. (2022) [50]	2.5D-based cascaded multi-stage framework (DS-CMSF)	LUNA16 dataset; LIDC-IDRI dataset	95.95% sensitivity and 89.50% CPM for nodule detection. 86.75% DSC for nodule segmentation.	Proposed a 2.5D cascaded multi-stage framework achieving a balance between accuracy and complexity.	DSC (Dice Similarity Coefficient); CPM (Competition Performance Metric); FOM (Figure of Merit)
Han et al. (2022) [51]	Pulmonary Nodules Detection Assistant Platform (3D CNN for detection)	LNPE1000 dataset; LUNA16 dataset	On LNPE1000: 0.879 detection accuracy, comparable to human experts.	Designed a dedicated CAD platform for physical examination LDCT images, with a focus on optimizing the detection ability of small nodules.	Detection Accuracy (including true positives and true negatives)
Xu et al. (2023) [56]	Improved Faster R-CNN	LUNA16 dataset	Detection precision: increased from 76.4% to 90.7%; recall: increased from 40.1% to 56.8%.	Multi-scale training, low-dimensional feature path augmentation, Online Hard Example Mining (OHEM).	Precision; Recall

Table 2. Cont.

Author	Model	Dataset	Result	Core Innovations of the Study	Definition of Key Experimental Indicators
Song et al. (2024) [52]	Multiscale 3D anchor-free network (M3N)	LUNA16 dataset	CPM: 90.6%, exceeding state-of-the-art networks.	Proposed adjustable nodule modeling (ANM), Designed a point selection strategy (PSS).	CPM
Bhatia et al. (2024) [53]	Lightweight DNN	LUNA16 dataset	Accuracy: 98.2%; PSNR: 32.8%; SSIM: 0.97;	Weakly supervised dense instance segmentation (WDSI), Deep continuous learning (SS-CL), Lightweight architecture design.	Accuracy; PSNR (Peak Signal-to-Noise Ratio); SSIM (Structural Similarity Index)
Jiang et al. (2025) [45]	AI-CAD system	344 patients (from 2 hospitals)	Better subjective image quality (4.18 vs 3.63) and detection metrics. Detection accuracy: 98.32% in 1024 matrix	verifying the advantages of high-resolution matrices in detecting small nodules (<6 mm).	Subjective Image Quality Score; SNR (Signal-to-Noise Ratio)
Karimullah et al. (2024) [54]	CBO+DenseNet CNN	LIDC which contains 1135 annotated CT images	Accuracy: 98.17%; specificity: 97.32%; precision: 97.46%; recall: 97.89%	Colliding Bodies Optimization (CBO), Local Binary Pattern (LBP).	Accuracy; Specificity; Precision, Recall.
Lancaster et al. (2025) [59]	Commercially available AI software	1252 UKLS-baseline-CT-scans	NPV 92.0% (90.2–95.3%); classified one as negative; NPV: 99.8% (99.0–99.9%)	via high negative predictive value (NPV) to reduce the radiologists' workload.	NPV (Negative Predictive Value)
CAI et al. (2025) [57]	Yolov8-AH	LUNA16 dataset	mAP50 improved by 24%, precision improved by 8.2%	Adaptive gating sparse attention (AGSA), Haar wavelet downsampling (HWD).	mAP50 (mean Average Precision at Intersection over Union threshold of 50%)
Zamandoost et al. (2025) [58]	OMS-CNN	LUNA16 dataset; PN9 dataset	Sensitivity: 94.89%; CPM: 0.892	Proposed an optimized multi-scale CNN (OMS-CNN).	CPM; Sensitivity

#### 4. AI in CT Image-Based Lung Cancer Segmentation

The AI-assisted pulmonary nodule detection system can not only improve the pulmonary nodule detection rate but also extract the Region of Interest (ROI) through accurate segmentation and provide various qualitative and quantitative parameters. These parameters help physicians conduct more accurate quantitative assessments of pulmonary nodules and reduce the workload caused by large volumes of medical images [61]. Primakov et al. presented a fully automated pipeline for the detection and volumetric segmentation of non-small cell lung cancer (NSCLC), which was developed and validated on 1328 thoracic CT scans; physicians preferred automatic segmentations in 56% of the cases [48].

Currently, many deep learning segmentation models have been applied to the segmentation of lung tumor regions. Dong et al. [62] proposed a multi-view secondary input residual (MVSIR) convolutional neural network, and the Dice coefficient of this method for 3D segmentation of pulmonary nodules on the LIDC-IDRI dataset reached 0.926. Suzuki et al. introduced an improved 3D U-Net model for the automatic detection and segmentation of pulmonary nodules on chest CT images. Their adaptation enables reaching any feature map from the marginal output map in three steps, thereby preventing the gradient vanishing problem [63]. Bruntha et al. [64] developed a deep learning network called Lung\_PAYNet based on the pyramid attention mechanism. By enhancing the receptive field and optimizing spatial prediction capabilities, this network significantly improved the segmentation effect of small nodules, achieving a Dice coefficient of up to 95.7% on the LIDC-IDRI dataset and demonstrating excellent segmentation performance. Zhang et al. proposed a multi-scale segmentation squeeze-and-excitation UNet with a conditional random field (M-SegSEUNet-CRF) to automatically segment lung tumors from CT images. M-SegSEUNet-CRF can achieve a Dice coefficient of 0.851 on the internal dataset, presenting higher performance than 3D U-Net and its variants [65].

The manual detection and annotation of lung nodules by human experts is a time-consuming and inconsistent process [66]. Some deep learning models have shown great potential in both pulmonary nodule detection and lung tumor region segmentation, rather than being limited to a single task [67,68]. Several studies have successfully implemented multi-task learning [69,70], demonstrating the possibility of addressing these two aspects simultaneously. Banu et al. proposed a system comprising two cascaded stages: nodule detection based on a fine-tuned Faster R-CNN and nodule segmentation based on the U-Net architecture. The experimental results demonstrate that the proposed system yields a Dice score of 89.79% and 90.35% [71]. Zhou et al. proposed a 2.5D-based cascaded multi-stage framework for the automatic detection and segmentation (DS-CMSF) of pulmonary

nodules, which achieves 95.95% sensitivity and 89.50% CPM for nodule detection, and 86.75% DSC for nodule segmentation [50]. Dlamini et al. aimed to develop a fully automatic system that detects and segments pulmonary nodules using YOLOv4 and a region-based active contour model. The system consists of two main sections: detection and volumetric rendering [72]. A recent study explored the application of 3D U-Net architectures combined with Inception and ResNet modules for precise lung nodule detection through deep learning-based segmentation techniques. The ensemble of models achieved the highest average DSC of  $0.84 \pm 0.05$  [73].

A summary of the methods mentioned above is given in Table 3

**Table 3.** AI and CT image-based lung tumor segmentation methods.

Author	Model	Dataset	Segmentation Result	Core Innovations
Dong et al. (2020) [62]	Multi-view secondary input residual (MV-SIR) convolutional neural network	LIDC-IDRI dataset	Dice coefficient: 0.926, Average surface distance: 0.072	Converts 3D lung nodule segmentation into voxel classification by inputting multi-view.
Primakov et al. (2022) [48]	Fully automated pipeline for NSCLC detection and volumetric segmentation	1328 thoracic CT scans from 8 institutions	achieved an average DSC of 0.82 (IQR = 0.14)	Develops a fully automated pipeline for detection and segmentation of non-small cell lung cancer (NSCLC).
Suzuki et al. (2022) [63]	Modified three-dimensional (3D) U-net deep-learning model	LIDC-IDRI dataset, 89 unused chest CT scans, 450 chest CT scans	- Internal validation CPM: 94.7%; - External validation CPM: 83.3%	Optimizes the 3D U-net architecture for automated lung nodule detection and segmentation.
Zhang et al. (2022) [65]	Multi-scale segmentation squeeze-and-excitation UNet with conditional random field (M-SegSEUNet-CRF)	759 lung cancer CT scans, NSCLC-Radiomics and LIDC datasets	- Dice coefficient: 0.851 - IoU: 0.747 - Sensitivity: 0.827 - PPV: 0.900	Employs a multi-scale strategy, Embeds segmentation SE blocks (spatially adaptive attention) in 3D UNet, Adds dense connected Conditional Random Field.
Bruntha et al. (2022) [64]	Lung PAYNet (pyramidal attention-based deep learning network)	LIDC-IDRI dataset	Dice similarity coefficient: 95.7%, mIOU: 91.75%, Sensitivity: 92.57%, Precision: 96.75%	Designs encoder with inverted residual blocks and swish activation, Adds a feature pyramid attention network.
Banu et al. (2021) [71]	AWEU-Net (Attention-Aware Weight Excitation U-Net)	LUNA16 dataset; LIDC-IDRI dataset	- LUNA16: Dice score 89.79%, IoU 82.34%; - LIDC-IDRI: Dice score 90.35%, IoU 83.21%	Proposes a two-stage cascaded system: fine-tuned Faster R-CNN + AWEU-Net.
Zhou et al. (2022) [50]	2.5D-based cascaded multi-stage framework (DS-CMSF)	LUNA16 dataset; LIDC-IDRI dataset	Segmentation DSC: 0.8675; LUNA16 detection: 95.95% sensitivity, 89.50% CPM	Four-stage cascaded design: Yolov5 rough localization, candidate nodule selection, 3D fusion classification, 3D UNet.
DLAMINI et al. (2023) [72]	Fully automatic system	QIN lung CT dataset; LIDC-IDRI dataset	Dice score: 92.19% Precision: 96.57%, Sensitivity: 97.02%, F1: 96.79%	Integrates YOLOv4 and region-based active contour model for end-to-end processing. Adds 3D reconstruction and validation against 3D printed tumors.
Rikhari, H., et al. (2024) [73]	Ensemble of 3D U-Net models	Retrospective dataset from AIIMS Delhi; 53 CT scans	DSC (avg): $0.84 \pm 0.05$ ; IoU (avg): $0.74 \pm 0.06$ ; Reduces false positives (2.69–3.39)	Trains four individual 3D U-Net variants and fuses them into an ensemble, Uses a hybrid loss function.

## 5. AI in CT Image-Based Assessment of the Malignant Risk of Pulmonary Nodules

On the basis of achieving accurate segmentation and detection of pulmonary nodules, some studies have further focused on developing a pulmonary nodule malignant risk assessment system, aiming to provide clinicians with more reliable clinical decision-making support. The CNN model proposed by Massion et al. [74] can distinguish between benign and malignant pulmonary nodules, with an AUC of 0.921 in internal validation on the NLST dataset. Benign and malignant pulmonary nodules are illustrated in Figure 3.

Masood et al. [75] introduced an advanced multi-dimensional region-based fully convolutional network (mRFCN), which is specifically designed for the detection and classification of pulmonary nodules. Their model adopts a multi-layer fused region proposal network (mLRPN), aiming to enhance ROI selection by combining position-sensitive score maps. Heuvelmans et al. [76] developed the LCP-CNN model, which achieved an overall AUC of 94.5% (95% Confidence Interval (CI): 92.6–96.1) for identifying benign nodules in the test set. Its high sensitivity enables 22.1% of nodules to be ruled out for malignancy, thus avoiding unnecessary re-examinations. Liu et al. developed a self-supervision pre-training-based fine-grained network for predicting the malignancy of subsolid pulmonary nodules (SSPNs). The pre-trained model was established using data from the NLST and LUNA databases. The model's performance in the internal testing set was as follows: AUC, 0.964 (95% CI: 0.942–0.986); accuracy, 0.934 [77]. Zhang et al. introduced a deep learning framework that integrates U-Net-based segmentation and ResNet-based classification processes. Feature combination blocks are applied to facilitate

information sharing between the segmentation and classification components [78]. Zhao proposed the sequential multi-instance learning (SMILE) framework to predict high-risk lung cancer patients using multiple CT scans. SMILE includes two steps: a nodule detection algorithm with image category transformation and nodule malignancy prediction [79]. Wang et al. proposed a novel high-precision bilevel optimization method (HBOM) to search for an optimal 3D pulmonary nodule classification model. The model employed memory optimization techniques to reduce memory overhead. The results showed that NAS-HBO achieved an impressive accuracy of 91.51% [80]. Jin et al. introduced a MTST model for feature extraction, designed with a multi-task layer that simultaneously outputs benign-malignant binary classification, multi-level classification, and a detailed analysis of pulmonary nodule features. MTST achieved an accuracy of 93.24% in the binary classification of benign and malignant nodules [81].

In addition to classifying pulmonary nodules as benign or malignant, some studies focus on distinguishing malignant nodules from nodules associated with other conditions. In Ibrahim et al.'s study, a multi-classification deep learning model for diagnosing COVID-19, pneumonia, and lung cancer from a combination of chest X-ray and CT images is proposed [82]. Zhou et al. proposed an ensemble multi-view 3D convolutional neural network (EMV-3D-CNN) model to study the risk stratification of lung adenocarcinoma. The model achieves state-of-the-art performance, with AUCs of 91.3% and 92.9% for the diagnosis of benign/malignant and pre-invasive/invasive nodules, respectively [83]. Du et al. proposed a fusion feature-based pulmonary nodule classification method that fuses radiomics features with deep learning neural network features, aiming to automatically classify different types of pulmonary nodules. The AUCs for the tasks of classifying Calcification, Lobulation, Margin, Spiculation, Texture, and Malignancy reached 0.9663, 0.8113, 0.8815, 0.8140, 0.9010, and 0.9316, respectively [84].

A summary of the methods mentioned above is given in Table 4.

**Table 4.** CT image-based methods for distinguishing benign from malignant pulmonary nodules.

Author	Model	Dataset	Classification Result	Involves Technologies	Core Innovations
Massion et al. (2020) [74]	Convolutional Neural Network	NLST dataset; Validation dataset:116 nodules	- External validation AUCs: 83.5% and 91.9%	classification	Focuses on indeterminate pulmonary nodules (IPNs); Validates across multiple cohorts.
Masood et al. (2020) [75]	Enhanced multidimensional region-based FCN (mRFCN)	LIDC dataset	- Detection sensitivity: 98.1% - Benign-malignant classification accuracy: 97.91%	detection classification	Integrates mLRPN with position-sensitive score maps; Adds deconvolutional layer to optimize region of interest selection.
Ibrahim et al. (2021) [82]	VGG19-CNN	chest X-ray and CT datasets obtained around 33,676 images	Accuracy: 98.05%, Recall: 98.05%, Precision: 98.43%, Specificity: 99.5%, F1 score: 98.24%, AUC: 99.66%	classification	Combines chest X-ray and CT images, Compares four deep learning architectures.
Heuvelmans et al. (2021) [76]	Lung Cancer Prediction Convolutional Neural Network (LCP-CNN)	NLST datasets; LUCINDA study (2106 nodules)	AUC: 94.5% sensitivity:99.0%, ruling out malignancy in 22.1% of nodules	classification	Sets a high-sensitivity threshold to minimize missed cancers, focuses on ruling out benign nodules.
Zhou et al. (2023) [83]	Ensemble multi-view 3D convolutional neural network (EMV-3D-CNN)	1075 lung nodules ( $\leq 30$ mm, $\geq 4$ mm)	- Benign/malignant classification AUC: 91.3% - Invasive adenocarcinoma grade classification Accuracy: 77.6%	classification	Uses ensemble multi-view 3D-CNN to capture comprehensive nodule features. Implements a web-based system.
Liu et al. (2024) [77]	Self-supervision pre-training-based fine-grained network	NLST, LUNA16; Internal: 1389; External: 202;	AUC 0.945, Accuracy 0.911, Sensitivity 0.977, Specificity 0.860	classification	Targets sub centimeter solid pulmonary nodules (SSPNs), Uses large-scale self-supervised pre-training
Zhang et al. (2025) [78]	Detection-guided model	LUNA16 dataset; the small dataset: 56 lesions	- Segmentation: Dice score 0.814, HD 3.188 mm, - Classification: Sensitivity 0.885	detection, segmentation, classification	Combines U-Net and ResNet with feature combination blocks Uses classification results as priors to refine segmentation.
Zhao et al. (2025) [79]	Sequential Multi-Instance Learning (SMILE)	925-patient dataset (182 malignant, 743 benign)	AUROC: 0.833, AUPRC: 0.740, Accuracy: 0.797, F1score: 0.777	detection classification	leverage temporal changes for malignancy prediction; Eliminates nodule location annotation by using multi-instance learning.
Wang et al. (2025) [80]	Neural Architecture Search with High-Precision Bilevel Optimization (NAS-HBO)	LIDC-IDRI dataset	Classification accuracy: 91.51%	classification	Automates 3D nodule classification model design via NAS-HBO. Adds Maintaining Receptive Field Criterion (MRFC).

Table 3. Cont.

Author	Model	Dataset	Classification Result	Involves Technologies	Core Innovations
Du et al. (2025) [84]	Fusion feature model (radiomics features + deep learning features)	LIDC-IDRI dataset	AUCs: Calcification 0.9663, Lobulation 0.8113, Margin 0.8815, Spiculation 0.8140, Texture 0.9010, Malignancy 0.9316	classification	Fuses radiomics and deep learning features; Addresses class imbalance by improving recognition of minority nodule types.
Jin et al. (2025) [81]	Multitask Swin Transformer (MTST)	LIDC-IDRI dataset	Classification: 93.74% accuracy, 91.55% sensitivity, Multi classification: accuracy: 95.73%	classification	Designs a multitask layer, Uses U-Net Generative Adversarial Network for image augmentation. Employ Swin Transformer to capture global and local nodule features.

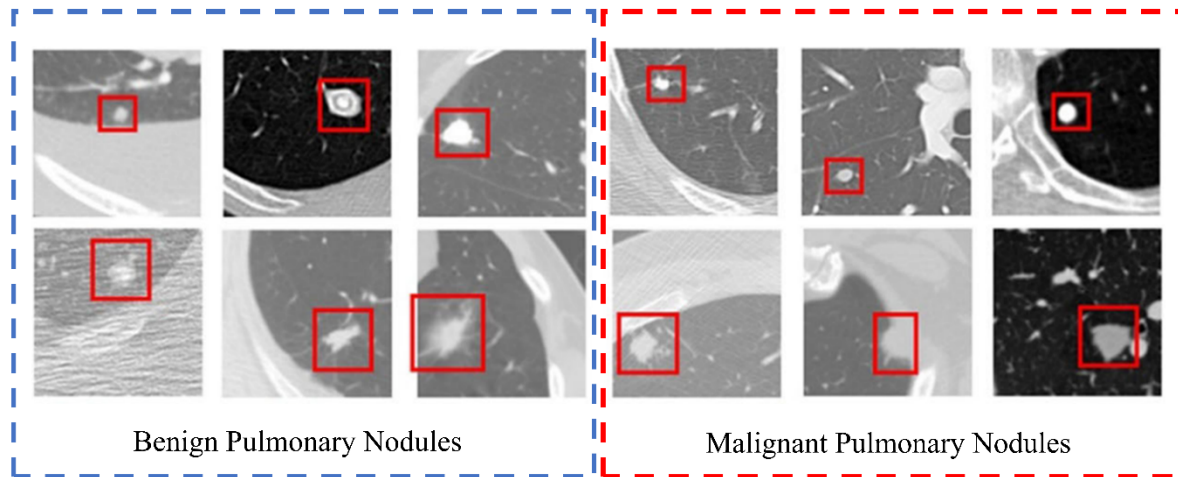


Figure 3. Display of benign and malignant pulmonary CT nodule image samples.

## 6. AI in CT Image-Based Prediction of Targeted Gene Mutations in Lung Cancer

Even lung tumors of the same pathological subtype may exhibit significant differences at the molecular level, leading to varying responses to treatment. With the development of targeted therapy, the non-invasive identification of patients with tumor gene mutations has become crucial. Currently, there are several studies on predicting the phenotypic mutation status of epidermal growth factor receptor (EGFR) based on CT images. Wang et al. constructed an effective deep learning model for predicting EGFR mutations from CT images, achieving favorable predictive performance in both the training set (AUC = 0.85) and the validation set (AUC = 0.81) [85]. de Margerie-Mellon et al. used radiological features to predict the EGFR phenotype in a cohort of 353 lung adenocarcinoma cases, obtaining an AUC of 0.69 [86]. Instead of focusing solely on tumor features, Wang et al. further extracted whole-lung information from CT images for EGFR prediction, and their model achieved an AUC ranging from 0.748 to 0.813 across six retrospective and prospective test cohorts [87]. Zhao et al. proposed a Denseformer framework to identify EGFR mutation status in a real end-to-end fashion directly from 3D lung CT images. The framework takes 3D whole-lung CT images as input to the neural network model without the need for manual labeling of lung nodules [88].

Meanwhile, some studies have integrated multi-modal data to enable models to predict EGFR mutation status more accurately. Xiao used the advanced EfficientNet-V2 model to predict EGFR mutations based on fused PET/CT images, where each individual PET and CT image was fused. The model achieved a prediction accuracy of 81.92% for distinguishing EGFR-mutated from non-EGFR-mutated cases in a cohort of 150 patients [89]. Kim et al. combined deep learning and radiomics to predict EGFR mutations in patients with non-small cell lung cancer (NSCLC) using computed tomography (CT) images. A total of 1280 NSCLC patients were enrolled in the final study. By integrating radiomics and clinical features, the external validation dataset yielded an area under the curve (AUC) of 0.7038 [90]. Lu et al. proposed LUCID, a multimodal data integration framework designed to predict EGFR mutation status and survival outcomes in lung cancer patients. LUCID leverages lung computed tomography (CT) images, chief complaints, laboratory test results, and demographic data to deliver non-invasive predictions. The model achieved strong performance in a cohort of 5175 patients, with AUCs ranging from 0.851 to 0.881 for EGFR mutation prediction [91].

In addition to independently predicting EGFR mutation status, some studies have achieved the prediction of multiple lung cancer-related mutation statuses. Dong et al. proposed a multi-channel and multi-task deep learning (MMDL) model for the simultaneous prediction of EGFR and Kirsten Rat Sarcoma Viral Oncogene Homolog (KRAS) mutation statuses based on CT images [92]. Hinzpeter et al. built two statistical models to evaluate the predictive ability of [<sup>18</sup>F]-FDG PET/CT-derived radiomics features for driver gene mutations in NSCLC. Overall, 55% of tumor samples demonstrated a mutation in TP53, 26% of samples had alterations in KRAS, and 17% had alterations in EGFR [93].

A summary of the methods mentioned above is given in Table 5.

**Table 5.** CT image-based methods for predicting lung cancer-related gene mutation status.

Author	Model	Dataset	Prediction Result	Genes Predicted	Imaging Modality	Core Innovations
Wang et al. (2019) [85]	End-to-end deep learning model	844 lung adenocarcinoma patients (2 hospitals)	- Primary cohort (n = 603): AUC 0.85 - validation cohort (n = 241): AUC 0.81	EGFR	CT	Proposes non-invasive EGFR mutation prediction using CT, Focuses on lung adenocarcinoma.
Dong et al. (2021) [92]	Multi-channel multi-task deep learning (MMDL) model	363 patients (partner hospital); 162 patients (TCIA public dataset)	- Training accuracy: EGFR 79.43%, KRAS 72.25% - Validation accuracy: EGFR 75.06%, KRAS 69.64%	EGFR; KRAS	CT	Enables simultaneous prediction of EGFR and KRAS mutations; Uses multi-channel views. Integrates patient personal information.
Wang et al. (2022) [87]	Fully automated artificial intelligence system (FAIS)	18,232 lung cancer patients	- EGFR genotype prediction AUC: 0.748–0.813 (6 testing cohorts)	EGFR	CT	Uses whole-lung CT information Predicts both EGFR genotype and EGFR-TKI treatment response; Validates across diverse cohorts.
Xiao et al. (2023) [89]	EfficientNet-V2 model (PET/CT fusion)	150 NSCLC patients	- Training accuracy: 86.25% - Validation accuracy: 81.92%	EGFR	PET/CT	Fuses PET and CT images for multi-modal feature integration., Uses EfficientNet-V2 for efficient, high-performance feature learning.
Zhao et al. (2024) [88]	Denseformer framework	Lung adenocarcinoma dataset (173 patients)	EGFR mutation prediction AUC 0.807, ACC 0.801	EGFR	CT	Combines CNN and Transformer in Denseformer. Uses whole-lung CT to capture tumour-microenvironment associations with EGFR mutations.
KIM et al. (2024) [90]	Deep learning–radiomics integrated model	1410 NSCLC patients;	Internal AUC: 0.81, External AUC: 0.78, External validation AUC 0.7038	EGFR	CT	Integrates deep learning features and radiomics features for complementary information, Includes clinical data.
Hinzpeter et al. (2024) [93]	Radiogenomics models	128 NSCLC patients	Youden Index: TP53 0.70, KRAS 0.57, EGFR: 0.60	EGFR; KRAS; TP53	[ <sup>18</sup> F]-FDG PET/CT	Uses [ <sup>18</sup> F]-FDG PET/CT radiomics to predict multiple driver mutations (EGFR, KRAS, TP53).
Lu et al. (2025) [91]	LUCID (multimodal data integration framework)	Retrospective cohort: 5175 lung cancer patients	EGFR mutation prediction AUC: 0.851–0.881; Survival time prediction AUC: 0.821–0.912	EGFR	CT	Fuses multimodal data for comprehensive prediction, Predicts both EGFR mutation status and patient survival outcomes (dual clinical value).

## 7. Discussion

This study conducts a statistical analysis of deep learning models related to lung cancer diagnosis based on CT images in recent years. This review emphasizes the important role of artificial intelligence (AI), particularly deep learning methods, in chest CT image diagnosis. Recent studies have demonstrated the significant potential of AI-based methods applied to chest CT images in improving the accuracy and efficiency of lung cancer screening and benign-malignant differentiation.

First, this study summarizes and describes public datasets related to CT-based lung cancer diagnosis, with a detailed analysis of the specific data volume and imaging modalities of each dataset. Subsequently, it conducts an

in-depth analysis of the specific fields in which deep learning methods have been applied to CT-based lung cancer diagnosis research. In lung cancer screening, detection algorithms such as YOLO and Faster R-CNN have been applied to pulmonary nodule detection on chest CT images, leading to significant breakthroughs in screening procedures. Specifically, AI can effectively identify suspicious pulmonary nodules in chest CT scans; however, further improvements to the models are still required to reduce false positives. In lung cancer segmentation tasks, the goal is to segment tumor regions and identify relevant imaging biomarkers in lung cancer patients by analyzing these segmented regions. Improved methods based on the U-Net segmentation model have greatly enhanced the accuracy of tumor region segmentation. Meanwhile, several studies have developed automated systems that enable models to simultaneously perform pulmonary nodule detection and segmentation tasks. Building on the aforementioned two tasks, AI has been applied to the benign-malignant classification of lung cancer. A number of deep learning models can effectively distinguish between benign and malignant nodules with considerable accuracy. In addition to the above applications, AI has also been used in lung cancer gene mutation analysis. It has been proven that AI can assist physicians in determining the status of genetic biomarkers through CT images. Particularly for EGFR and KRAS gene mutations, several studies have shown that deep learning models can capture subtle morphological changes in tumors caused by gene mutations. This capability allows for the identification of lung cancer-related gene mutation status based on CT images, thereby better guiding the development of personalized treatment plans for lung cancer patients.

However, in the field of artificial intelligence (AI)-assisted lung cancer diagnosis technology, the translation of technologies from theoretical laboratory research to clinical practice still requires overcoming numerous obstacles and faces many pressing challenges. Among these, dataset limitations, medical data privacy concerns, and insufficient model interpretability have become core bottlenecks restricting their clinical adoption, severely impeding the implementation of these technologies in real-world medical settings.

### 7.1. Dataset Limitations

Most of the current research on relevant models conducts experiments and validation based on public datasets with high-quality annotations. By virtue of their openness, public datasets provide researchers with abundant sample information and a solid research foundation, playing a vital role in the early stage of technology development. Nevertheless, the inherent limitations of public datasets are quite prominent: on one hand, their data sources often fail to cover the diversity of different regions, populations, and disease subtypes, making it impossible to fully ensure the consistency of imaging data quality; on the other hand, some public datasets have a limited sample size and may suffer from issues such as outdated data collection methods and disconnection from current real-world clinical diagnosis and treatment scenarios, leading to insufficient data representativeness. Models trained on such datasets often struggle to maintain stable performance when confronted with complex cases in real clinical settings. Meanwhile, some models perform well in controlled laboratory environments, but once applied to real clinical scenarios, their diagnostic efficiency and accuracy decrease significantly when facing complex factors such as differences in data distribution, varying equipment models, and individual patient variations—failing to meet the clinical requirements for robustness.

### 7.2. Medical Data Privacy

A series of issues including medical data privacy protection, diagnostic safety, and model robustness further exacerbate the difficulties in the clinical application of these technologies. In the research and development as well as clinical application of AI models for lung cancer imaging, data privacy protection is one of the core challenges. Particularly, the CT data relied on by lung cancer imaging AI models contains a wealth of sensitive information, and privacy leakage will trigger serious ethical and legal risks. Therefore, how to balance model efficiency and data privacy has become a crucial issue in this field. The innovative application of technologies such as Federated Learning (FL) and Private Blockchain provides an effective solution to this problem.

Adnan et al. [94] proposed a lung cancer prediction model that constructs an integrated framework combining MapReduce, Private Blockchain, Federated Learning (FL), and Explainable Artificial Intelligence (XAI). Among them, Federated Learning enables multiple medical institutions to collaboratively train models without sharing raw CT data, effectively avoiding the risk of patient privacy leakage; MapReduce technology addresses the high computing power demand for large-scale medical data processing, endowing the model with both efficiency and privacy security. Ultimately, the diagnostic accuracy of this model in lung cancer prediction reaches 98.21%. Meanwhile, Chen et al. [95] combined meta-learning with Federated Learning and proposed a robust model based on multi-center CT imaging datasets for diagnosing tuberculous granulomas and lung adenocarcinomas in solitary pulmonary solid nodules (SPSNs). Each institution does not need to upload raw CT data or clinical data, but only

trains local model parameters based on local data, and then aggregates global features through Federated Learning—this not only protects data privacy but also solves the problem of model overfitting caused by the limited sample size of a single hospital. The Area Under the Curve (AUC) of this model in different cohort test sets ranges from 0.808 to 0.927.

These two studies demonstrate that privacy-preserving technologies can not only address the dilemma of difficult medical data sharing but also enhance the generalization ability and clinical applicability of AI models for lung cancer imaging. Models based on Federated Learning can break down data silos, as they can not only utilize massive multi-center data to improve model generalization ability but also strictly safeguard patient privacy. This provides a scalable paradigm for privacy protection and performance optimization of lung cancer AI models, promoting their advancement toward clinical practicality.

### 7.3. Model Interpretability

With the gradual increase in the depth and structural complexity of model networks, although the fitting ability and diagnostic accuracy of the models have been improved, this also poses significant challenges to model interpretability. The lack of interpretability further undermines the credibility of models in clinical applications—since the derivation basis of diagnostic conclusions cannot be clearly presented, clinicians struggle to determine whether model decisions rely on key medical features or are disturbed by irrelevant noise. This leads to insufficient trust in model results, making it difficult to truly integrate the models into the diagnosis and treatment process. Currently, existing interpretation methods (such as heatmaps) can mostly only reveal local information in the model decision-making process, but fail to fully reflect the complex nonlinear operation mechanisms and decision-making logic within the models. They can neither trace the complete transmission path of features from input to output nor explain the interactions between multiple features.

In addition, current research rarely involves the performance of models under adversarial conditions, and this issue is particularly critical in high-risk fields such as medical imaging. Adversarial examples refer to samples that cause models to make incorrect judgments on images that were originally correctly diagnosed by artificially adding tiny noises imperceptible to the human eye. Due to the extremely high requirements for detail accuracy in medical images, the interference of tiny noises may directly alter diagnostic conclusions. However, existing models not only lack the ability to resist such adversarial interference but also have not established effective adversarial detection and defense mechanisms. Under the deep learning framework, there are significant differences in the performance of mainstream models for lung cancer CT diagnosis (such as CNN and Transformer) under adversarial conditions. These differences stem from the image feature extraction logic of the two types of models and need to be thoroughly analyzed in combination with the characteristics of model architectures. From the perspective of CNN (Convolutional Neural Network) models, they rely on local convolution kernels and pooling layers to gradually extract image features. This structure causes them to exhibit the characteristics of local perturbation amplification when exposed to adversarial examples. In contrast, Transformer models can globally capture the correlations between image pixels through the self-attention mechanism, theoretically having stronger robustness to local noises. However, adversarial examples can interfere with the attention weight allocation of Transformers, making the models shift their attention from real lesions to irrelevant regions. In multi-model combined lung cancer diagnosis systems, differences in the adversarial vulnerability of individual models may also lead to contradictory diagnostic results, losing clinical reference value. Once adversarial examples are encountered in practical clinical applications, they will not only result in misdiagnosis and missed diagnosis but also may trigger medical disputes, posing a serious threat to patients' life and health. This research gap has also become an important bottleneck restricting the practical application of artificial intelligence in lung cancer CT diagnosis.

### 7.4. Limitations of This Study

Although this paper explicitly focuses on the application of deep learning methods in CT-based lung cancer diagnosis and conducts precise discussions around model methods in this specific field, it still has significant limitations. Firstly, the research scope is confined to the diagnostic phase and does not extend to the extended level of clinical practice after diagnosis. Regarding how to formulate personalized and precise treatment plans based on patients' individual differences after lung cancer diagnosis, this paper lacks corresponding analysis and explanation. This results in insufficient integrity of the research outcomes in clinical translation, making it difficult to directly support subsequent treatment decisions. Secondly, as a key consideration for the application of deep learning in the medical field, model interpretability is only roughly summarized in this paper without more detailed and in-depth discussions. Deep learning models often suffer from insufficient interpretability, and the transparency of their diagnostic logic and feature extraction processes directly affects clinicians' trust and willingness to apply

them. However, this paper does not conduct in-depth analysis of this core pain point nor propose effective improvement ideas, leading to insufficient practicality and persuasiveness of the research. It fails to fully respond to the dual demands for model reliability and interpretability in the medical field.

## 8. Conclusions

AI-assisted lung cancer diagnosis has gradually moved from laboratory research to clinical practice. Its characteristics of precision, efficiency, and personalization endow it with high application value and broad prospects. Meanwhile, in the process of the deep integration of clinical artificial intelligence with the medical field—promoting the integration of clinical data, genetic data, radiological imaging data, and histopathological data—the boundaries of AI-assisted decision-making need to be clearly defined. This ensures that while medical experts use AI to simplify a large number of information-intensive and time-consuming manual tasks, they can still play a leading role in critical decision-making. Only in this way can the AI-assisted lung cancer diagnosis system more effectively mine useful information from massive amounts of data, thereby assisting medical experts in making more informed diagnosis and treatment decisions.

## Author Contributions

B.Z.: Conceptualization, methodology, data curation, investigation, writing—original draft; Y.W.: Methodology, formal analysis, writing—review and editing. All authors have read and agreed to the published version of the manuscript.

## Funding

This research was funded by General Program of Zhejiang Provincial Department of Education (Grant No. Y202559701) and Innovation Team Project of the Ningbo Yongjiang Talent Program (Grant No. ZX2025000419).

## Institutional Review Board Statement

Not applicable.

## Informed Consent Statement

Not applicable.

## Data Availability Statement

Not applicable.

## Conflicts of Interest

The authors declare no conflict of interest.

## Use of AI and AI-Assisted Technologies

During the preparation of this work, the authors used DeepSeek to understanding of technical concepts and Polish the wording. After using this tool, the authors reviewed and edited the content as needed and takes full responsibility for the content of the published article.

## References

1. Bray, F.; Laversanne, M.; Sung, H.; et al. Global cancer statistics 2022: GLOBOCAN estimates of incidence and mortality worldwide for 36 cancers in 185 countries. *CA Cancer J. Clin.* **2024**, *74*, 229–263.
2. The, L. Lung cancer treatment: 20 years of progress. *Lancet* **2024**, *403*, 2663.
3. Han, B.; Zheng, R.; Zeng, H.; et al. Cancer incidence and mortality in China, 2022. *J. Natl. Cancer Cent.* **2024**, *4*, 47–53.
4. Schabath, M.B.; Cote, M.L. Cancer Progress and Priorities: Lung Cancer. *Cancer Epidemiol. Biomarkers Prev.* **2019**, *28*, 1563–1579.
5. Nicholson, A.G.; Tsao, M.S.; Beasley, M.B.; et al. The 2021 WHO Classification of Lung Tumors: Impact of Advances Since 2015. *J. Thorac. Oncol.* **2022**, *17*, 362–387.
6. Kanwal, M.; Ding, X.J.; Cao, Y. Familial risk for lung cancer. *Oncol. Lett.* **2017**, *13*, 535–542.
7. Panunzio, A.; Sartori, P. Lung Cancer and Radiological Imaging. *Curr. Radiopharm.* **2020**, *13*, 238–242.

8. Migliore, M.; Palmucci, S.; Nardini, M.; et al. Imaging patterns of early stage lung cancer for the thoracic surgeon. *J. Thorac. Dis.* **2020**, *12*, 3349–3356.
9. Li, N.; Tan, F.; Chen, W.; et al. One-off low-dose CT for lung cancer screening in China: A multicentre, population-based, prospective cohort study. *Lancet Respir. Med.* **2022**, *10*, 378–391.
10. Lancaster, H.L.; Heuvelmans, M.A.; Oudkerk, M. Low-dose computed tomography lung cancer screening: Clinical evidence and implementation research. *J. Intern. Med.* **2022**, *292*, 68–80.
11. de Koning, H.J.; van der Aalst, C.M.; de Jong, P.A.; et al. Reduced Lung-Cancer Mortality with Volume CT Screening in a Randomized Trial. *N. Engl. J. Med.* **2020**, *382*, 503–513.
12. Henschke, C.I.; Yip, R.; Salvatore, M.; et al. The Regimen of Computed Tomography Screening for Lung Cancer: Lessons Learned Over 25 Years from the International Early Lung Cancer Action Program. *J. Thorac. Imaging* **2021**, *36*, 6–23.
13. Nihashi, T.; Matsuura, N.; Kawamata, T.; et al. Monitoring of fatigue in radiologists during prolonged image interpretation using fNIRS. *JPN J. Radiol.* **2019**, *37*, 437–448.
14. Klang, E. Deep learning and medical imaging. *J. Thorac. Dis.* **2018**, *10*, 1325–1328.
15. Lawson, C.E.; Marti, J.M.; Radivojevic, T.; et al. Machine learning for metabolic engineering: A review. *Metab. Eng.* **2021**, *63*, 34–60.
16. Hwang, E.J.; Park, C.M. Clinical Implementation of Deep Learning in Thoracic Radiology: Potential Applications and Challenges. *Korean J. Radiol.* **2020**, *21*, 511–525.
17. Warraich, H.J.; Tazbaz, T.; Califf, R.M. FDA Perspective on the Regulation of Artificial Intelligence in Health Care and Biomedicine. *JAMA* **2025**, *333*, 241–247.
18. Zhang, H.; Wang, L.; Li, X.; et al. The application of artificial intelligence in lung cancer: A narrative review. *Transl. Cancer Res.* **2021**, *10*, 2478–2487.
19. Bidzinska, J.; Szurowska, E. See Lung Cancer with an AI. *Cancers* **2023**, *15*, 1321.
20. Adams, S.J.; Bredin, A.; Ireland, A.; et al. Lung cancer screening. *Lancet* **2023**, *401*, 390–408.
21. Goncalves, S.; Fong, P.C.; Blokhina, M.; et al. Artificial intelligence for early diagnosis of lung cancer through incidental nodule detection in low- and middle-income countries-acceleration during the COVID-19 pandemic but here to stay. *Am. J. Cancer Res.* **2022**, *12*, 1–16.
22. Manafi-Farid, R.; Ataei, G.; Pirich, C.; et al. [<sup>18</sup>F]FDG-PET/CT Radiomics and Artificial Intelligence in Lung Cancer: Technical Aspects and Potential Clinical Applications. *Semin. Nucl. Med.* **2022**, *52*, 759–780.
23. Lu, S.Y.; Zhu, Z.; Zhang, Y.D.; et al. Tuberculosis and pneumonia diagnosis in chest X-rays by large adaptive filter and aligning normalized network with report-guided multi-level alignment. *Eng. Appl. Artif. Intell.* **2025**, *158*, 111576.
24. Lu, S.Y.; Zhu, Z.; Tang, Y.; et al. CTBViT: A novel ViT for tuberculosis classification with efficient block and randomized classifier. *Biomed. Signal Process. Control* **2025**, *100*, 106981.
25. Zhu, Z.; Liu, L.; Free, R.C.; et al. OPT-CO: Optimizing pre-trained transformer models for efficient COVID-19 classification with stochastic configuration networks. *Inf. Sci.* **2024**, *680*, 121141.
26. Zhu, Z.; Lu, S.Y.; Huang, T.; et al. LKA: Large Kernel Adapter for Enhanced Medical Image Classification. In *International Conference on Medical Image Computing and Computer-Assisted Intervention*; Springer: Cham, Switzerland, 2025.
27. Kalchier-Dekel, O.; Connolly, J.G.; Lin, I.H.; et al. Shape-Sensing Robotic-Assisted Bronchoscopy in the Diagnosis of Pulmonary Parenchymal Lesions. *Chest* **2022**, *161*, 572–582.
28. Zheng, X.; He, B.; Hu, Y.; et al. Diagnostic Accuracy of Deep Learning and Radiomics in Lung Cancer Staging: A Systematic Review and Meta-Analysis. *Front. Public Health* **2022**, *10*, 938113.
29. Mao, Y.; Xu, N.; Wu, Y.; et al. Assessments of lung nodules by an artificial intelligence chatbot using longitudinal CT images. *Cell Rep. Med.* **2025**, *6*, 101988.
30. Niu, C.; Guo, Y.; Tian, S.; et al. Medical multimodal multitask foundation model for lung cancer screening. *Nat. Commun.* **2025**, *16*, 1523.
31. Guo, J.; Miao, J.; Sun, W.; et al. Predicting bone metastasis-free survival in non-small cell lung cancer from preoperative CT via deep learning. *NPJ Precis. Oncol.* **2024**, *8*, 161.
32. Chiu, H.-Y.; Chao, H.-S.; Chen, Y.-M. Application of artificial intelligence in lung cancer. *Cancers* **2022**, *14*, 1370.
33. Kotoulas, S.C.; Spyrtos, D.; Porpodis, K.; et al. A Thorough Review of the Clinical Applications of Artificial Intelligence in Lung Cancer. *Cancers* **2025**, *17*, 882.
34. Huang, J.; Xiang, Y.; Gan, S.; et al. Application of artificial intelligence in medical imaging for tumor diagnosis and treatment: A comprehensive approach. *Discov. Oncol.* **2025**, *16*, 1–23.
35. Ayasa, Y.; Alajrami, D.; Idkedek, M.; et al. The Impact of Artificial Intelligence on Lung Cancer Diagnosis and Personalized Treatment. *Int. J. Mol. Sci.* **2025**, *26*, 8472.
36. Armato, S.G., III; McLennan, G.; Bidaut, L.; et al. The Lung Image Database Consortium (LIDC) and Image Database Resource Initiative (IDRI): A completed reference database of lung nodules on CT scans. *Med. Phys.* **2011**, *38*, 915–931.

37. Hosny, A.; Parmar, C.; Coroller, T.P.; et al. Deep learning for lung cancer prognostication: A retrospective multi-cohort radiomics study. *PLoS Med.* **2018**, *15*, e1002711.
38. Black, W.C.; Keeler, E.B.; Soneji, S.S. Cost-effectiveness of CT screening in the National Lung Screening Trial. *N. Engl. J. Med.* **2015**, *372*, 388.
39. Setio, A.A.A.; Traverso, A.; de Bel, T.; et al. Validation, comparison, and combination of algorithms for automatic detection of pulmonary nodules in computed tomography images: The LUNA16 challenge. *Med. Image Anal.* **2017**, *42*, 1–13.
40. de Margerie-Mellon, C.; Chassagnon, G. Artificial intelligence: A critical review of applications for lung nodule and lung cancer. *Diagn. Interv. Imaging* **2023**, *104*, 11–17.
41. Cellina, M.; Ce, M.; Irmici, G.; et al. Artificial Intelligence in Lung Cancer Screening: The Future Is Now. *Cancers* **2023**, *15*, 4290.
42. Gu, D.; Liu, G.; Xue, Z. On the performance of lung nodule detection, segmentation and classification. *Comput. Med. Imaging Graph.* **2021**, *89*, 101886.
43. Li, L.; Liu, Z.; Huang, H.; et al. Evaluating the performance of a deep learning-based computer-aided diagnosis (DL-CAD) system for detecting and characterizing lung nodules: Comparison with the performance of double reading by radiologists. *Thorac. Cancer* **2019**, *10*, 183–192.
44. Duranti, L.; Ceccarelli, L.; Milano, M.; et al. New Perspectives on Lung Cancer Screening and Artificial Intelligence. *Life* **2025**, *15*, 498.
45. Jiang, Q.; Wang, Y.; Zhang, T.; et al. High-resolution computed tomography with 1024-matrix for artificial intelligence-based computer-aided diagnosis in the evaluation of pulmonary nodules. *J. Thorac. Dis.* **2025**, *17*, 289–298.
46. Jiang, Q.; Sun, H.; Deng, W.; et al. Super Resolution of Pulmonary Nodules Target Reconstruction Using a Two-Channel GAN Models. *Acad. Radiol.* **2024**, *31*, 3427–3437.
47. Park, S.; Lee, S.M.; Kim, W.; et al. Computer-aided Detection of Subsolid Nodules at Chest CT: Improved Performance with Deep Learning-based CT Section Thickness Reduction. *Radiology* **2021**, *299*, 211–219.
48. Primakov, S.P.; Wu, G.; Ibrahim, A.; et al. Automated detection and segmentation of non-small cell lung cancer computed tomography images. *Nat. Commun.* **2022**, *13*, 3423.
49. Liu, W.; Liu, X.; Li, H.; et al. Integrating Lung Parenchyma Segmentation and Nodule Detection with Deep Multi-Task Learning. *IEEE J. Biomed. Health Inform.* **2021**, *25*, 3073–3081.
50. Zhou, Z.; Gou, F.; Tan, Y.; et al. A Cascaded Multi-Stage Framework for Automatic Detection and Segmentation of Pulmonary Nodules in Developing Countries. *IEEE J. Biomed. Health Inform.* **2022**, *26*, 5619–5630.
51. Han, Y.; Qi, H.; Wang, L.; et al. Pulmonary nodules detection assistant platform: An effective computer aided system for early pulmonary nodules detection in physical examination. *Comput. Methods Programs Biomed.* **2022**, *217*, 106680.
52. Song, W.; Tang, F.; Marshall, H.; et al. A multiscale 3D network for lung nodule detection using flexible nodule modeling. *Med. Phys.* **2024**, *51*, 7356–7368.
53. Bhatia, I.; Aarti; Ansarullah, S.I.; et al. Lightweight Advanced Deep Neural Network (DNN) Model for Early-Stage Lung Cancer Detection. *Diagnostics* **2024**, *14*, 2356.
54. Karimullah, S.; Khan, M.; Shaik, F.; et al. An integrated method for detecting lung cancer via CT scanning via optimization, deep learning, and IoT data transmission. *Front. Oncol.* **2024**, *14*, 1435041.
55. Huang, Y.S.; Chou, P.R.; Chen, H.M.; et al. One-stage pulmonary nodule detection using 3-D DCNN with feature fusion and attention mechanism in CT image. *Comput. Methods Programs Biomed.* **2022**, *220*, 106786.
56. Xu, J.; Ren, H.; Cai, S.; et al. An improved faster R-CNN algorithm for assisted detection of lung nodules. *Comput. Biol. Med.* **2023**, *153*, 106470.
57. Cai, J.; Wang, L.; Cai, J.; et al. Contactless Intelligent Anti-interference Lung Nodule Detection Method for Early Disease Detection. *IEEE J. Biomed. Health Inform.* **2025**, 1–12. <https://doi.org/10.1109/JBHI.2025.3550199>.
58. Zamanidoost, Y.; Ould-Bachir, T.; Martel, S. OMS-CNN: Optimized Multi-Scale CNN for Lung Nodule Detection Based on Faster R-CNN. *IEEE J. Biomed. Health Inform.* **2025**, *29*, 2148–2160.
59. Lancaster, H.L.; Jiang, B.; Davies, M.P.A.; et al. Histological proven AI performance in the UKLS CT lung cancer screening study: Potential for workload reduction. *Eur. J. Cancer* **2025**, *220*, 115324.
60. Jarnalo, C.O.M.; Linsen, P.V.M.; Blazis, S.P.; et al. Clinical evaluation of a deep-learning-based computer-aided detection system for the detection of pulmonary nodules in a large teaching hospital. *Clin. Radiol.* **2021**, *76*, 838–845.
61. Gao, J.; Qi, Q.; Li, H.; et al. Artificial-intelligence-based computed tomography histogram analysis predicting tumor invasiveness of lung adenocarcinomas manifesting as radiological part-solid nodules. *Front. Oncol.* **2023**, *13*, 1096453.
62. Dong, X.; Xu, S.; Liu, Y.; et al. Multi-view secondary input collaborative deep learning for lung nodule 3D segmentation. *Cancer Imaging* **2020**, *20*, 53.

63. Suzuki, K.; Otsuka, Y.; Nomura, Y.; et al. Development and Validation of a Modified Three-Dimensional U-Net Deep-Learning Model for Automated Detection of Lung Nodules on Chest CT Images from the Lung Image Database Consortium and Japanese Datasets. *Acad. Radiol.* **2022**, *29*, S11–S17.
64. Bruntha, P.M.; Pandian, S.I.A.; Sagayam, K.M.; et al. Lung\_PAYNet: A pyramidal attention based deep learning network for lung nodule segmentation. *Sci. Rep.* **2022**, *12*, 20330.
65. Zhang, B.; Qi, S.; Wu, Y.; et al. Multi-scale segmentation squeeze-and-excitation UNet with conditional random field for segmenting lung tumor from CT images. *Comput. Methods Programs Biomed.* **2022**, *222*, 106946.
66. Erasmus, J.J.; Gladish, G.W.; Broemeling, L.; et al. Interobserver and intraobserver variability in measurement of non-small-cell carcinoma lung lesions: Implications for assessment of tumor response. *J. Clin. Oncol.* **2003**, *21*, 2574–2582.
67. Kim, H.; Goo, J.M.; Lee, K.H.; et al. Preoperative CT-based Deep Learning Model for Predicting Disease-Free Survival in Patients with Lung Adenocarcinomas. *Radiology* **2020**, *296*, 216–224.
68. Ohno, Y.; Aoyagi, K.; Yaguchi, A.; et al. Differentiation of Benign from Malignant Pulmonary Nodules by Using a Convolutional Neural Network to Determine Volume Change at Chest CT. *Radiology* **2020**, *296*, 432–443.
69. Hunter, B.; Chen, M.; Ratnakumar, P.; et al. A radiomics-based decision support tool improves lung cancer diagnosis in combination with the Herder score in large lung nodules. *EBioMedicine* **2022**, *86*, 104344.
70. Gugulothu, V.K.; Balaji, S. An early prediction and classification of lung nodule diagnosis on CT images based on hybrid deep learning techniques. *Multimed. Tools Appl.* **2023**, *83*, 12571–12591.
71. Banu, S.F.; Sarker, M.M.K.; Abdel-Nasser, M.; et al. AWEU-Net: An Attention-Aware Weight Excitation U-Net for Lung Nodule Segmentation. *Sci. Rep.* **2021**, *11*, 10132.
72. Dlamini, S.; Chen, Y.-H.; Kuo, C.-F.J. Complete fully automatic detection, segmentation and 3D reconstruction of tumor volume for non-small cell lung cancer using YOLOv4 and region-based active contour model. *Expert Syst. Appl.* **2023**, *212*, 118661.
73. Rikhari, H.; Baidya Kayal, E.; Ganguly, S.; et al. Improving lung nodule segmentation in thoracic CT scans through the ensemble of 3D U-Net models. *Int. J. Comput. Assist. Radiol. Surg.* **2024**, *19*, 2089–2099.
74. Massion, P.P.; Antic, S.; Ather, S.; et al. Assessing the Accuracy of a Deep Learning Method to Risk Stratify Indeterminate Pulmonary Nodules. *Am. J. Respir. Crit. Care Med.* **2020**, *202*, 241–249.
75. Masood, A.; Sheng, B.; Yang, P.; et al. Automated Decision Support System for Lung Cancer Detection and Classification via Enhanced RFCN With Multilayer Fusion RPN. *IEEE Trans. Ind. Inform.* **2020**, *16*, 7791–7801.
76. Heuvelmans, M.A.; van Ooijen, P.M.A.; Ather, S.; et al. Lung cancer prediction by Deep Learning to identify benign lung nodules. *Lung Cancer* **2021**, *154*, 1–4.
77. Liu, J.; Qi, L.; Xu, Q.; et al. A Self-supervised Learning-Based Fine-Grained Classification Model for Distinguishing Malignant from Benign Subcentimeter Solid Pulmonary Nodules. *Acad. Radiol.* **2024**, *31*, 4687–4695.
78. Zhang, J.; Yang, M.; Guo, W.; et al. Detection-guided deep learning-based model with spatial regularization for lung nodule segmentation. *Quant. Imaging Med. Surg.* **2025**, *15*, 4204–4216.
79. Zhao, W.; Liao, W.; Tang, Y.; et al. Lung Cancer Screening Classification by Sequential Multi-Instance Learning (SMILE) Framework with Multiple CT Scans. *IEEE Trans. Med. Imaging* **2025**, *44*, 3151–3161.
80. Wang, M.; Gu, Y.; Yang, L.; et al. A novel high-precision bilevel optimization method for 3D pulmonary nodule classification. *Phys. Med.* **2025**, *133*, 104954.
81. Jin, H.; Yu, C.; Zhang, J.; et al. Multitask Swin Transformer for classification and characterization of pulmonary nodules in CT images. *Quant. Imaging Med. Surg.* **2025**, *15*, 1845–1861.
82. Ibrahim, D.M.; Elshennawy, N.M.; Sarhan, A.M. Deep-chest: Multi-classification deep learning model for diagnosing COVID-19, pneumonia, and lung cancer chest diseases. *Comput. Biol. Med.* **2021**, *132*, 104348.
83. Zhou, J.; Hu, B.; Feng, W.; et al. An ensemble deep learning model for risk stratification of invasive lung adenocarcinoma using thin-slice CT. *NPJ Digit. Med.* **2023**, *6*, 119.
84. Du, L.; Tang, G.; Che, Y.; et al. Fusing radiomics and deep learning features for automated classification of multi-type pulmonary nodule. *Med. Phys.* **2025**, *52*, e17901.
85. Wang, S.; Shi, J.; Ye, Z.; et al. Predicting EGFR mutation status in lung adenocarcinoma on computed tomography image using deep learning. *Eur. Respir. J.* **2019**, *53*, 1800986.
86. de Margerie-Mellon, C.; Gill, R.R.; Salazar, P.; et al. Assessing invasiveness of subsolid lung adenocarcinomas with combined attenuation and geometric feature models. *Sci. Rep.* **2020**, *10*, 14585.
87. Wang, S.; Yu, H.; Gan, Y.; et al. Mining whole-lung information by artificial intelligence for predicting EGFR genotype and targeted therapy response in lung cancer: A multicohort study. *Lancet Digit. Health* **2022**, *4*, e309–e319.
88. Zhao, S.; Li, W.; Liu, Z.; et al. End-to-End Prediction of EGFR Mutation Status with Denseformer. *IEEE J. Biomed. Health Inform.* **2024**, *28*, 54–65.
89. Xiao, Z.; Cai, H.; Wang, Y.; et al. Deep learning for predicting epidermal growth factor receptor mutations of non-small cell lung cancer on PET/CT images. *Quant. Imaging Med. Surg.* **2023**, *13*, 1286–1299.

90. Kim, S.; Lim, J.H.; Kim, C.H.; et al. Deep learning–radiomics integrated noninvasive detection of epidermal growth factor receptor mutations in non-small cell lung cancer patients. *Sci. Rep.* **2024**, *14*, 922.
91. Lu, Y.; Liu, F.; Yu, Y.; et al. AI-enabled molecular phenotyping and prognostic predictions in lung cancer through multimodal clinical information integration. *Cell Rep. Med.* **2025**, *6*, 102216.
92. Dong, Y.; Hou, L.; Yang, W.; et al. Multi-channel multi-task deep learning for predicting EGFR and KRAS mutations of non-small cell lung cancer on CT images. *Quant. Imaging Med. Surg.* **2021**, *11*, 2354–2375.
93. Hinzpeter, R.; Kulanthaivelu, R.; Kohan, A.; et al. Predictive [<sup>18</sup>F]-FDG PET/CT-Based Radiogenomics Modelling of Driver Gene Mutations in Non-small Cell Lung Cancer. *Acad. Radiol.* **2024**, *31*, 5314–5323.
94. Adnan, K.M.; Ghazal, T.M.; Saleem, M.; et al. Secure and interpretable lung cancer prediction model using mapreduce private blockchain federated learning and XAI. *Sci. Rep.* **2025**, *15*, 35693.
95. Chen, Y.; Liu, L.; Feng, B.; et al. A meta-learning-based robust federated learning for diagnosing lung adenocarcinoma and tuberculosis granulomas. *Front. Oncol.* **2025**, *15*, 1666937.